Received: 22 July 2016 | Revised: 15 September 2016 | Accepted: 20 September 2016

DOI 10.1002/aoc.3663

WILEY Applied Organometallic Chemistry

FULL PAPER

A route to magnetically separable nanocatalysts: Combined experimental and theoretical investigation of alkyl substituent role in ligand backbone towards epoxidation ability

Tanmay Chattopadhyay[1] | Aratrika Chakraborty[2] | Sanchari Dasgupta[2] | Arnab Dutta[2] | M. Isabel Menéndez[3] | Ennio Zangrando[4]

[1] Department of Chemistry, Panchakot Mahavidyalaya, Sarbari, Purulia 723 121, India

[2] Department of Chemistry, University of Calcutta, 92 A. P. C. Road, Kolkata 700 009, India

[3] Departamento de Química Física y Analítica, Universidad de Oviedo, C/ Julián Clavería 8, 33006 Oviedo, Spain

[4] Dipartimento di Scienze Chimiche, University of Trieste, Via L. Giorgieri 1, 34127 Trieste, Italy

Correspondence
Tanmay Chattopadhyay, Department of Chemistry, Panchakot Mahavidyalaya, Sarbari, Purulia 723 121, India.
Email: tanmayc2003@gmail.com
M. Isabel Menéndez, Departamento de Química Física y Analítica, Universidad de Oviedo, C/ Julián Clavería 8, 33006 Oviedo, Spain.
Email: isabel@uniovi.es
Ennio Zangrando, Dipartimento di Scienze Chimiche, University of Trieste, Via L. Giorgieri 1, 34127 Trieste, Italy.
Email: ezangrando@units.it

Funding information
Science and Engineering Research Board, Grant/Award Number: SB/FT/CS-185/2013 dt. 30-06-2014.

We have prepared two chiral Schiff base ligands, H_2L^1 and H_2L^2, and one achiral Schiff base ligand, H_2L^3, by treating 2,6-diformyl-4-methylphenol separately with (*R*)-1,2-diaminopropane, (*R*)-1,2-diaminocyclohexane and 1,1′-dimethylethylenediamine, in ethanolic medium, respectively. The complexes MnL^1ClO_4 (**1**), MnL^2ClO_4 (**2**), MnL^3ClO_4 (**3**), FeL^1ClO_4 (**4**), FeL^2ClO_4 (**5**) and FeL^3ClO_4 (**6**) have been obtained by reacting the ligands H_2L^1, H_2L^2 and H_2L^3 with manganese(III) perchlorate or iron (III) perchlorate in methanol. Circular dichroism studies suggest that ligands H_2L^1 and H_2L^2 and their corresponding complexes have asymmetric character. Complexes **1–6** have been used as homogeneous catalysts for epoxidation of alkenes. Manganese systems have been found to be much better than iron counterparts for alkene epoxidation, with **3** as the best catalyst among manganese systems and **6** as the best among iron systems. The order of their experimental catalytic efficiency has also been rationalized by theoretical calculations. We have observed higher enantiomeric excess product with catalysts **1** and **4**, so they were attached to surface-modified magnetic nanoparticles to obtain two new magnetically separable nanocatalysts, Fe_3O_4@dopa@MnL^1 and Fe_3O_4@dopa@FeL^4. They have been characterized and their alkene epoxidation ability has been investigated. These catalysts can be easily recovered by magnetic separation and recycled several times without significant loss of catalytic activity. Hence our study focuses on the synthesis of a magnetically recoverable asymmetric nanocatalyst that finds applications in epoxidation of alkenes and at the same time can be recycled and reused.

KEYWORDS

asymmetric complex, catalysis, epoxidation, magnetic nanoparticles, recyclable

1 | INTRODUCTION

Catalysis is a broad field which has already been deeply studied in specific areas but still leaves much scope for the development of catalytic systems at different levels. Thus research in this field remains significant in the area of chemical sciences and allied branches. Epoxides are versatile intermediates in organic chemistry that can constitute convenient building blocks for the synthesis of many commodity and fine chemicals.[1,2] Numerous studies have focused on the preparation of epoxides using transition metal salen complexes in the presence of terminal oxidants, e.g. iodosylbenzene (PhIO), NaOCl and H_2O_2.[3] The extensive use of metal salen complexes in homogeneous catalysis can be attributed to their high activity, selectivity and enantioselectivity (when chiral complexes are used).[4–7] The easy availability of active sites of homogeneous catalysts enhances their efficiency, but their liability lies in the difficulty in their separation from reaction mixtures. Alternatively, for heterogeneous catalysts simple separation techniques are available, although lower catalytic activity may be seen due to the difficulty of accessing the active sites.

It is obvious that a catalyst system having the advantageous attributes of both homogeneous and heterogeneous systems would be highly desirable. In this line of thinking, magnetically separable nanocatalysts emerge as an adequate solution, as has been recently reported.[8–10] Magnetic separation is simple, ecological and allows easy recycling of the catalyst.[9–14] Besides, magnetically separable nanocatalysts also offer excellent surface-to-volume ratio, which enhances the contact between reactants and catalyst, which increases the overall activity of the catalyst for the desired transformations.

Several research groups have recently investigated steric and electronic effects of manganese and non-heme iron complexes on alkene epoxidations,[15] and our own research team has given a deeper insight into the effect of halogen substituents at the ligand backbone of Schiff base Fe(III) complexes on epoxide yield.[7] The relevance of the topic encourages us to delve further, by exploring the effect of alkyl groups at the non-aromatic chain of the ligands. For this purpose we have selected three Mn(III) and three Fe(III) Schiff base complexes, as shown in Scheme 1, among which **2** and **5** had been previously synthesized and tested as catalysts for the epoxidation of olefins in the presence of PhIO in CH_3CN under mild conditions.[16,17] They are included in the present work for the sake of completeness due to their close relationship with the four new catalysts here analysed. Further, theoretical calculations helped us to rationalize the experimental catalytic efficiency of the whole set of catalysts. Also, in the work presented here we devised a technique to attach some selected manganese and iron catalyst complexes to surface-modified nanoparticles in order to build efficient, stable and easy-to-recover magnetically separable nanocatalysts. To summarize our work, we have designed an efficient magnetically separable asymmetric nanocatalyst for alkene epoxidation that maintains its activity even after several catalytic cycles, hence solving the problems of tedious separation procedure of heterogeneous catalysts.

2 | EXPERIMENTAL

2.1 | Materials and methods

All chemicals were purchased from commercial sources and used as received. Solvents were dried according to standard procedures and distilled prior to use. Iodosylbenzene was prepared according to a literature method.[16]

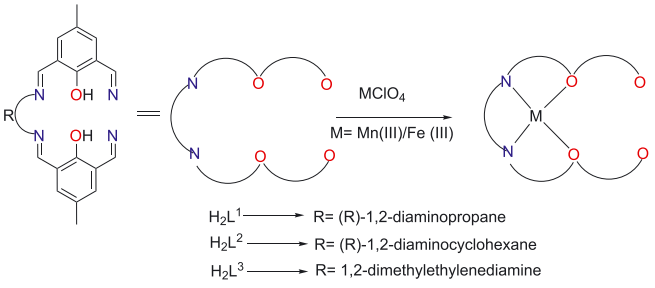

SCHEME 1 Schematic representation of the preparation of metal–Schiff base complexes

2.2 | Syntheses

2,6-Diformyl-4-methylphenol was prepared according to a literature method.[16] Schiff bases H_2L^1, H_2L^2 and H_2L^3 were prepared by reacting 2,6-diformyl-4-methylphenol separately with (*R*)-1,2-diaminopropane, (*R*)-1,2-diaminocyclohexane and 1,1′-dimethylethylenediamine, in ethanolic medium in 2:1 ratio. All the complexes were synthesized and characterized according to the same procedure as previously reported.[16,17] Very similar analytical results were also observed for **5** as earlier described.[17]

2.2.1 | [MnL^1ClO_4] (1)

Yield: 88% (with respect to L^1). Anal. calcd (%): C, 48.62; H, 3.89; N, 5.40. Found (%): C, 48.58; H, 3.84; N, 5.45. IR (KBr, ν, cm^{-1}): ν(C=O) 1655, ν(C=N) 1626, ν(skeletal vibration) 1545, $\nu(ClO_4)$ 1109. UV (λ_{max}(MeOH), nm): 422 (sh, ε = 7300 dm^3 mol^{-1} cm^{-1}), 360 (ε = 10 000 dm^3 mol^{-1} cm^{-1}). MS (ESI positive mode): *m/z* (%) = 418.92 (100) $[M]^+$.

2.2.2 | [MnL^2ClO_4] (2)

Yield: 85% (with respect to L^2). Anal. calcd (%): C, 51.58; H, 4.33; N, 5.01. Found (%): C, 51.38; H, 4.30; N, 5.11. IR (KBr, ν, cm^{-1}): ν(C=O) 1660, ν(C=N) 1624, ν(skeletal vibration) 1547, $\nu(ClO_4)$ 1112. UV (λ_{max}(MeOH), nm): 412 (sh, ε = 7500 dm^3 mol^{-1} cm^{-1}), 360 (ε = 15 000 dm^3 mol^{-1} cm^{-1}). MS (ESI positive mode): *m/z* (%) = 459.12 (100) $[M]^+$.

2.2.3 | [MnL^3ClO_4] (3)

Yield: 84% (with respect to L^3). Anal. calcd (%): C, 49.59; H, 4.16; N, 5.26. Found (%): C, 49.53; H, 4.14; N, 5.30. IR (KBr, ν, cm^{-1}): ν(C=O) 1657, ν(C=N) 1624, ν(skeletal vibration) 1548, $\nu(ClO_4)$ 1103. UV (λ_{max}(MeOH), nm): 422 (sh, ε = 7600 dm^3 mol^{-1} cm^{-1}), 360 (ε = 14 300 dm^3 mol^{-1} cm^{-1}). MS (ESI positive mode): *m/z* (%) = 433.12 (100) $[M]^+$.

2.2.4 | [FeL^1ClO_4] (4)

Yield: 84% (with respect to L^1). Anal. calcd (%): C, 48.55; H, 3.85; N, 5.39. Found (%): C, 49.01; H, 4.02; N, 5.30. IR (KBr, ν, cm^{-1}): ν(C=O) 1660, ν(C=N) 1632, ν(skeletal vibration) 1548, $\nu(ClO_4)$ 1104. UV (λ_{max}(MeOH), nm): 526 (sh, ε = 5600 dm^3 mol^{-1} cm^{-1}), 330 (ε = 12 300 dm^3 mol^{-1} cm^{-1}). MS (ESI positive mode): *m/z* (%) = 685.48 (100) $[M + 4CH_3OH + 6Na]^+$.

2.2.5 | [FeL^3ClO_4] (6)

Yield: 86% (with respect to L^3). Anal. calcd (%): C, 49.51; H, 4.15; N, 5.25. Found (%): C, 49.53; H, 4.14; N, 5.30. IR (KBr, ν, cm^{-1}): ν(C=O) 1655, ν(C=N) 1628, ν(skeletal vibration) 1545, $\nu(ClO_4)$ 1100. UV (λ_{max}(MeOH), nm): 522

(sh,ε = 5500 dm^3 mol^{-1} cm^{-1}), 350 (ε = 8000 dm^3 mol^{-1} cm^{-1}). MS (ESI positive mode): m/z (%) = 434.22 (100) [M]$^+$.

2.2.6 | Preparations of Fe_3O_4-NPs, Fe_3O_4@dopa, Fe_3O_4@dopa@MnL^1 and Fe_3O_4@dopa@FeL^1

Fe_3O_4-NPs and Fe_3O_4@dopa were prepared following the same procedure as we reported earlier.[7] Fe_3O_4@dopa@MnL^1 and Fe_3O_4@dopa@FeL^1 were synthesized with a slightly modified procedure than before: 1 g of FeL^{1}ClO$_4$ or MnL^{1}ClO$_4$ was added to a dispersed acetonitrile solution of Fe_3O_4@dopa (500 mg). The mixture was stirred for 10 h at room temperature. The product was allowed to settle, washed several times with acetonitrile and dried under vacuum at 60°C for 2 h. For Fe_3O_4@dopa@MnL^1: ν_1(C═N) 1626 cm^{-1}; ν_2(C═N) 1655 cm^{-1}; ν(skeletal vibration) 1531 cm^{-1}; ν(Fe_3O_4) 577 cm^{-1}. For Fe_3O_4@dopa@FeL^1: ν_1(C═N) 1621 cm^{-1}; ν_2(C═N) 1645 cm^{-1}; ν(skeletal vibration) 1537 cm^{-1}; ν(Fe_3O_4) 589 cm^{-1}.

2.3 | 1.3 Characterization

Elemental analyses (carbon, hydrogen and nitrogen) were performed using a PerkinElmer 240C elemental analyser. Fourier transform infrared (FT-IR) spectra (500–4000 cm^{-1}) were recorded at 27°C using a PerkinElmer RXI FT-IR spectrophotometer with KBr pellets. Electronic spectra (200–800 nm) were obtained at 27°C using a Shimadzu UV-3101PC with methanol as solvent and reference. Thermal analyses were carried out with a Mettler Toledo (TGA/SDTA851) thermal analyser in flowing dinitrogen (flow rate: 30 cm^3 min^{-1}). Electrospray mass spectra were recorded with a MICROMASS Q-TOF mass spectrometer. Field emission scanning electron microscopy (SEM) observation was carried out with a JEOL JSM-6700F field-emission microscope. The particle size and microstructure were studied using transmission electron microscopy (TEM) with a JEOL (Japan) JEM 2100 high-resolution transmission electron microscope operating at 200 kV. Powder X-ray diffraction (PXRD) spectra were recorded at room temperature using an XPERT-PRO diffractometer with monochromated Cu Kα radiation (40.0 kV, 30.0 mA). A vibrating sample magnetometer (EV-9, Microsense, ADE) was utilized for obtaining the magnetization curves. Circular dichroism (CD) spectra were measured with a Jobin Ivon CD 6 spectrophotometer in acetonitrile.

2.4 | X-ray crystallography

Single-crystal data for **5** were collected at the X-ray diffraction beamline XRD1 of the Elettra Synchrotron, Trieste (Italy), using the rotating crystal method with a monochromatic wavelength of 0.7000 Å, using a Dectris Pilatus 2 M detector. Measurements were performed at 100(2) K using a nitrogen stream cryo-cooler. Cell refinement, indexing and scaling of the data set were performed using the CCP4 package,[18] and programs Denzo and Scalepack.[19] The structure was solved by direct methods and Fourier analyses and refined by full-matrix least-squares based on F2 with all observed reflections.[20] All non-hydrogen atoms were refined with anisotropic displacement coefficients. A disordered lattice ethanol molecule was fixed with half occupancy. Crystallographic data and details of refinement are provided in Table 1.

2.5 | Epoxidation study of catalysts 1–6

To a solution of alkene (0.30 mmol) in acetonitrile (15 ml), 0.01 mmol of the complex was added followed by addition of PhIO (0.30 mmol) portion-wise and then the resultant mixture was stirred at room temperature for 2 h in air. The reaction progress was monitored by TLC. After removal of solvent, the crude product was purified by flash chromatography. Identification of the epoxide was performed using ^{1}H NMR spectroscopy.

2.6 | Epoxidation study of Fe_3O_4@dopa@MnL^1 and Fe_3O_4@dopa@FeL^1

To a solution of alkene (2 mmol) in acetonitrile (15 ml), 100 mg of nanocatalyst was suspended followed by addition of PhIO (2 mmol) and the resultant mixture were stirred at room temperature for 2 h in air. PhIO was added portion-wise to the solution here as well. The reaction progress was monitored by TLC. After completion of the reaction, the catalyst was magnetically separated and the solvent was removed using a rotary evaporator. The crude product thus obtained was purified by flash chromatography. Identification of the epoxide was performed using ^{1}H NMR spectroscopy.

TABLE 1 Crystal data and details of refinement for complex **5**

Empirical formula	$C_{51}H_{65}Cl_2Fe_2N_4O_{21.50}$
Formula weight	1260.67
Crystal system, space group	Monoclinic, *C*2
a (Å)	20.1210(12)
b (Å)	10.2560(8)
c (Å)	28.6220(15)
β (°)	106.60(2)
Volume (Å^3)	5660.3(8)
Z, calculated density (Mg m^{-3})	4, 1.479
μ (mm^{-1})	0.610
F(000)	2628
θ range data collection (°)	1.46–29.98
Reflections collected / unique	48 408 / 16 945
R(int)	0.0232
Data / parameters	16945 / 767
Goodness-of-fit on F^2	1.054
Final *R* indices [$I > 2\sigma(I)$]	*R*1 = 0.0404, *wR*2 = 0.1106
R indices (all data)	*R*1 = 0.0413, *wR*2 = 0.1117
Residuals (e. Å^{-3})	1.124, −0.756

2.7 | Computational method

All calculations were carried out with the Gaussian 09 series of programs.[21] The implicit polarizable continuum model of Tomasi and co-workers[22,23] was used to take into account the effect of acetonitrile as solvent (dielectric constant $\varepsilon = 35.688$), using atomic radii derived from the standard universal force field. Full geometry optimization of all reactants and products was carried out using density functional theory with the UB3LYP[22,23] functional and the 6–311 + G(d,p) basis set for C, N, O and H atoms as well as with LANL2DZ pseudopotential for Mn and Fe atoms. This theory level has rendered accurate results in previous studies of related systems.[24,25] Geometry optimizations were done with the Schlegel algorithm.[26–28] The located stationary points were checked to be true minima by the analytical computation of the harmonic vibrational frequencies at the same theory level. Due to the open shell nature of the Mn and Fe complexes under study, the possible low- and high-spin states were calculated for non-oxidized and oxidized complexes. High-spin structures were found to be more stable than low-spin ones in all cases, and they showed practically no spin contamination at the theory level used here.

3 | RESULTS AND DISCUSSION

3.1 | Synthesis and characterization

Six purposely selected complexes have been prepared following a procedure slightly modified from our earlier reports.[16,17] Here Schiff bases H_2L^1, H_2L^2 and H_2L^3 have been prepared in ethanolic medium by treating 2,6-diformyl-4-methylphenol separately with (*R*)-1,2-diaminopropane, (*R*)-1,2-diaminocyclohexane and 1,1′-dimethylethylenediamine. Further treatment of H_2L^1, H_2L^2 and H_2L^3 with manganese(III) perchlorate gives complexes MnL^1 (**1**), MnL^2 (**2**) and MnL^3 (**3**), and on reaction with iron(III) perchlorate complexes FeL^1 (**4**), FeL^2 (**5**) and FeL^3 (**6**). Only complex 5 rendered single crystals suitable for X-ray diffraction. All the complexes have been characterized by standard physicochemical methods. We observed similar characteristic FT-IR bands in the ranges *ca* 1660–1670, *ca* 1610–1630 and *ca* 1500–1548 cm^{-1} assigned to C═O, C═N and skeletal vibrations for all the complexes, as we reported earlier for **2** and **5**.[16,17] We also found characteristic FT-IR bands at the range *ca* 1090–1110 cm^{-1} for perchlorate anion present in all the prepared complexes. Electronic absorption spectra of all the complexes in methanolic medium show various intense bands in the UV and visible regions as we reported earlier for **2** and **5** (Figure S1 and S2, supporting information).[16,17] CD measurements for all the complexes were also performed and their CD spectra are presented in Figure 1. As expected, **3** and **6** are CD inactive due to absence of chirality.

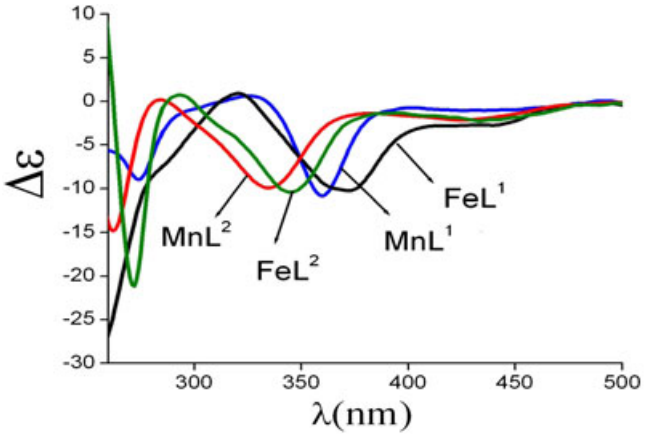

FIGURE 1 CD spectra of the chiral complexes MnL^1 (**1**), MnL^2 (**2**), FeL^1 (**4**) and FeL^2 (**5**)

The X-ray structure of FeL^2 complex is depicted in Figure 2. This structural analysis evidenced two crystallographically independent FeL^2 complexes (A, B) besides two perchlorate anions, and two ethanol molecules (one of which disordered at half occupancy) (Figure S3, supporting information). The two complexes slightly differ in their conformational geometry, although both metals exhibit an octahedral coordination environment comprising the tetradentate Schiff base and two aqua ligands at axial positions. The Fe—O (phenoxo) and Fe—N bond distances fall in the range 1.898 (2)–1.9030(18) and 2.084(2)–2.096(2) Å, respectively. On the other hand, a larger variation is observed in the Fe—OH_2 bond lengths that vary from 2.075(3) to 2.115(2) Å, likely modulated by the packing and the hydrogen bonds fashioned by the ligands. These data are in agreement with those found for similar salen-type $[Fe(L)(H_2O)_2]$ complexes previously reported.[29,30] The different conformation assumed by the chelating ligand in the two independent complexes A and B is noteworthy. For Fe1 in the A complex the equatorial coordination set N_2O_2 presents a slight tetrahedral distortion (displacement of ±0.12 Å), and thus the two chelating moieties (almost coplanar) are tilted forming a dihedral angle of 12.82°; for Fe2 in the B complex the ligand assumes a step

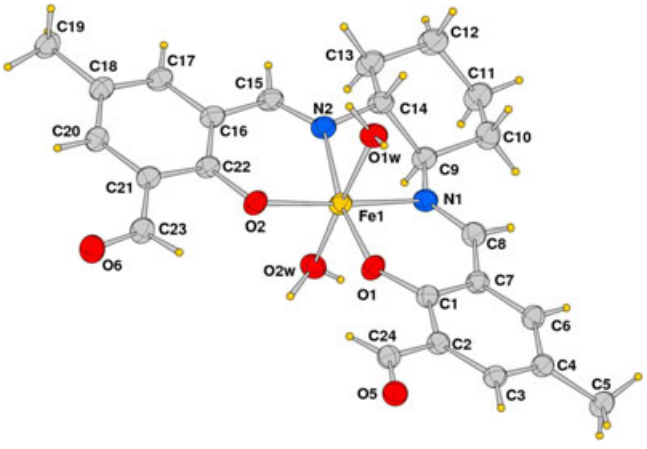

FIGURE 2 ORTEP drawing (50% probability ellipsoids) of the complex cation A of **5**

arrangement with the N_2O_2 coordination mean plane forming dihedral angles of 18.22° and 20.19° with the phenyl ring of each side, as displayed in Figure S4 (supporting information). The compound crystallizes in non-centrosymmetric space group *C*2 and the chelate ring formed by the 1,2-diaminocyclohexane fragment in both complexes presents δ chirality, with *R* configuration of both hexyl carbon atoms connected to the nitrogen donors. The complexes are arranged in pairs connected through hydrogen bonds occurring between the axial aqua ligands of one complex and the formyl oxygen atoms of the other, crystallographically related by a two-fold axis (Figure S5 and S6, supporting information). In addition each water molecule interacts through a hydrogen bond with ethanol oxygen or with a perchlorate anion. Selected coordination bond distances and angles for **5** are listed in Table S1 (supporting information). Hydrogen bond parameters are listed in Table S2 (supporting information). This packing leads the metals to be separated by 6.465 and 6.371 Å in the two A and B complex dimers. A similar structure with the formation of dimers in the solid state was detected in the manganese derivative with chloride: $[MnL^3(H_2O)_2]Cl$.[16]

3.2 | Optimization of conditions for catalytic epoxidation with PhIO

We have followed the same procedure for all homogeneous catalysed epoxidation reactions using catalysts **1**–**6**. In an initial experiment, (*Z*)-stilbene (0.30 mmol) (as representative), **2** (0.01 mmol) and PhIO (0.30 mmol) were mixed in 15 ml of acetonitrile and stirred for 2 h at room temperature. TLC was used to monitor the progress of the reaction. After usual work-up and chromatographic purification, the isolated epoxide yield was found to be 90%, which is very similar to that reported in our previous study.[16] To find the best catalytic conditions we kept 0.30 mmol of (*Z*)-stilbene whereas the catalyst amount was varied between 0.005 and 0.01 mmol, the amount of terminal oxidant, PhIO, between 0.25 and 0.35 mmol, and the reaction time between 1 and 3 h. We found that 0.01 mmol of catalyst **2**, 0.30 mmol of PhIO and 2 h reaction time provided the best yield. These optimum reaction conditions were applied to all homogeneously catalysed epoxidation reactions. The essential role played by the catalyst is evident from the extremely low (<2%) yield of epoxide found in a blank reaction carried out in the absence of the catalyst.

3.3 | Catalytic epoxidation of various alkenes with PhIO

Here we examined the epoxidation of three alkenes, (*E*)-stilbene, (*Z*)-stilbene or styrene, catalysed by complexes **1**–**6** in CH_3CN, with PhIO as terminal oxidant. Based on our previous studies,[7,16,17] we only consider CH_3CN as solvent. Table 2 presents the conversion, turnover number (TON) and isolated yield for the epoxidation of the alkenes. These data suggest some considerations. First, according to the reaction yields, manganese catalysts (yields between 78 and 92%) seem to be much more efficient than the corresponding iron ones (yields between 28 and 56%). Second, ligand L^3 gives rise to the highest yields with both metals (complexes **3** and **6**). Third, the effect of the various substituents at the backbone of the

TABLE 2 Epoxidation of alkenes catalysed by complexes **1**–**6** in CH_3CN with PhIO[a]

Catalyst	Substrate	Conversion (%)	TON[b]	Yield (%)[c]	ee (%)[d]
1	(*E*)-Stilbene	89	13.4	88	38
	(*Z*)-Stilbene	87	13.1	85 (*cis*: *trans* = 70: 30)	41
	Styrene	83	12.5	80	42
2	(*E*)-Stilbene	90	13.5	87	35
	(*Z*)-Stilbene	86	13.0	83 (*cis*: *trans* = 66: 34)	37
	Styrene	80	12.0	78	40
3	(*E*)-Stilbene	95	14.3	92	—
	(*Z*)-Stilbene	94	14.1	91 (*cis*: *trans* = 60: 40)	—
	Styrene	93	13.9	89	—
4	(*E*)-Stilbene	50	7.5	48	25
	(*Z*)-Stilbene	55	8.3	53 (*cis*: *trans* = 80: 20)	27
	Styrene	37	5.6	33	35
5	(*E*)-Stilbene	47	7.1	43	Trace[e]
	(*Z*)-Stilbene	51	7.7	49 (*cis*: *trans* = 70: 30)	Trace[e]
	Styrene	35	5.3	28	20
6	(*E*)-Stilbene	57	8.6	55	—
	(*Z*)-Stilbene	59	8.9	56 (*cis*: *trans* = 65: 35)	—
	Styrene	50	7.5	47	—

[a]Catalyst (0.01 mmol), alkene (0.30 mmol), PhIO (0.30 mmol) and CH_3CN (15 ml) stirred at room temperature for 2 h in air.

[b]TON = moles of substrate converted per mole of catalyst per hour.

[c]Isolated epoxide yield.

[d]Determined by ^1H NMR (300 Hz) in the presence of Eu(hfc). Configuration not determined.

[e]Concentration < 5%.

ligand is quite similar. Complexes **3** and **6** did not have chirality; thus we observed highest enantiomeric excess product for catalysts **1** and **4**. The order of the experimental catalytic efficiency has been rationalized by theoretical calculations, as explained below. The epoxidation process has also been monitored using UV–visible spectroscopy. We have obtained observations similar to those we reported earlier.[16,17] The results clearly suggests the generation of higher valent Mn^{V}═O and Fe^{V}═O species.

3.4 | Theoretical investigation

Initial Mn(III) complexes **1**–**3**, as well as Fe(III) ones discussed below, are assumed to be oxidized by PhIO ((a) in Figure S7, supporting information) to render the final oxidized Mn^{V}═O species, 1-oxo, 2-oxo and 3-oxo, and PhI ((b) in Figure S7, supporting information), along with two released water molecules. The complex oxidation schematically represented by the following equation is an intermediate step in the epoxidation of alkenes:

$$\text{Complex} + \text{PhIO} \Leftrightarrow \text{complex-oxo} + \text{PhI} \qquad (1)$$

Quantum chemical calculations were performed to see which catalysts render the most stable oxidized complexes, assuming that they have the best chance of providing higher epoxide yields.

Figure S8 (supporting information) displays the B3LYP/6–31 + G(d,p) optimized structures of the initial Mn(III) (with high, 5, and low, 3, spin multiplicity) and final Mn^{V}═O (with high, 3, and low, 1, spin multiplicity) complexes along with some selected geometrical parameters. For all initial Mn (III) complexes the metal ion is closer to oxygen atoms than to nitrogen ones in the equatorial plane. The hexacycle substituent of **2** makes both N atoms equivalent but the asymmetry caused by methyl and dimethyl substituents produces a slight enlargement of the Mn─N2 distance in **1** and **3**. Besides, the O─Mn─O angle (95°) is approximately 12° larger than the N─Mn─N one for all species. For the initial Mn complexes with high-spin multiplicity axial water ligands are about 2.36 Å apart from the metal but this distance reduces to 2.04 Å for low-spin multiplicity initial complexes. For the final Mn^{V}═O complexes the distance between Mn and axial oxygen is 1.641 and 1.53 Å, on average, for high- and low-spin complexes, respectively. Table S3 (supporting information) collects the absolute electronic and Gibbs energies of all these species in acetonitrile solution, and shows that high-spin complexes are more stable than low-spin ones for the initial and the final manganese complexes, although for the initial species the difference in Gibbs energy between both spin states is much larger (20.5 kcal mol^{-1} on average) than in the final ones (7.5 kcal mol^{-1} on average). Considering the most stable complexes, the spin multiplicity of the reaction would vary from 5 for the reactants to 3 for the oxidized Mn complexes, which is forbidden by the spin conservation rule. The only way such a reaction could happen would be through the assistance of another simultaneous reaction where the reverse spin change happened, that is, reactant spin multiplicity in the auxiliary reaction should be 3 and that of products 5. In this assumption, the Gibbs energy of the reaction in equation (1) is very similar for the three complexes with different substituents at the non-aromatic chain of the ligand, as displayed in the second column of Table S4 (supporting information). A small preference for the complex with two methyl substituents, **3**, is observed. The other reliable possibility for this oxidation to happen is the reaction taking place in the triplet state, which involves assuming that reactants are excited by about 20.5 kcal mol^{-1} to their triplet state before the beginning of the oxidation process. From this excited state they evolve to the stable triplet products. Last column in Table S4 (supporting information) indicates that, in this assumption, the complex with the cyclohexane substituent, **2**, is thermodynamically preferred, and closely followed by **3**, due to their most negative Gibbs reaction energy. It is interesting to note that the large energy released during the reaction at the triplet state can easily compensate the initial energy input needed to excite the reactants.

Figure S9 (supporting information) displays the B3LYP/6–31 + G(d,p) optimized structures of the initial Fe(III) (with high, 6, and low, 2, spin multiplicity) and final Fe^{V}═O (with high, 4, and low, 2, spin multiplicity) complexes along with some selected geometrical parameters. Compared to Mn complexes, initial Fe(III) ones could be described as shorter, due to smaller axial distances, and wider, due to larger equatorial distances. For all the initial iron complexes the metal is closer to oxygen atoms than to nitrogen ones in the equatorial plane. For those with high spin, the O─Fe─O angle (109°) is approximately 30° larger than the N─Fe─N one and axial water ligands are about 2.21 Å apart from the metal, but this distance reduces to 2.02 Å for low-spin ones. For the final Fe^{V}═O complexes the distance between Fe and axial oxygen is 1.610 Å and both O─Fe─O and N─Fe─N become of similar size (85° on average) for both spin multiplicities. Table S5 (supporting information) collects the absolute electronic and Gibbs energies of all these species in acetonitrile solution. As for Mn complexes, initial high-spin Fe complexes (spin multiplicity =6) are more stable than the low-spin ones (spin multiplicity =4), but now the difference between them amounts to 11 kcal mol^{-1} on average. However, final iron oxidized complexes present similar absolute energy, as previously reported for analogous systems.[7] It is noteworthy that theoretical geometry of **5** in the stable high-spin state is in agreement with experimental X-ray measurements previously discussed.

Table S6 (supporting information) shows that both mechanistic hypotheses previously explained (iron complex oxidation by PhIO happening assisted by an auxiliary reaction whose spin multiplicity changes from 4 to 6 or initial excitation of Fe complexes to a doublet state to yield products in a

doublet excited state) point to the complex with a dimethyl substituent at the non-aromatic chain of the ligand, **6**, as the most active one closely followed by **5**. Again, the large amount of energy released in the process taking place in the excited doublet state largely compensates the initial input of energy the complexes need to reach the doublet state (about 11 kcal mol^{-1}).

3.5 | Preparation and characterization of Fe_3O_4@dopa@MnL^1 and Fe_3O_4@dopa@FeL^1

A schematic diagram for the preparation of Fe_3O_4@dopa@MnL^1 and Fe_3O_4@dopa@FeL^1 is presented in Scheme 2. Magnetic nanoparticles Fe_3O_4 and modification of their surface were realized following the same procedure as we earlier reported.[7] For the preparation of Fe_3O_4@dopa@MnL^1 and Fe_3O_4@dopa@FeL^1, 1 g of MnL^1ClO_4 or FeL^1ClO_4 was added to a dispersed acetonitrile solution of amine-functionalized nano-Fe_3O_4 (Fe_3O_4@dopa, 500 mg), stirring the mixture for 14 h at room temperature. The product was allowed to settle, washed several times with acetonitrile and dried under vacuum at 50°C for 3 h. Newly prepared Fe_3O_4@dopa@MnL^1 and Fe_3O_4@dopa@FeL^1 were characterized as described in the following.

FT-IR spectra of MnL^1ClO_4, Fe_3O_4@dopa@MnL^1, FeL^1ClO_4, and Fe_3O_4@dopa@FeL^1 are presented in Figure 3. We observed very similar peaks for Fe_3O_4 and Fe_3O_4@dopa related to Fe—O bond and to the vibration of the benzene ring present in dopamine moiety.[7] Several new peaks are generated for Fe_3O_4@dopa@MnL^1 and Fe_3O_4@dopa@FeL^1, along with characteristic peaks as for Fe_3O_4. The peaks in the range 1530–1540 cm^{-1} may be assigned to the skeleton vibration of the complex. The sharp peaks in the ranges 1620–1626 and 1645–1660 cm^{-1} may be due to the presence of two types of C═N (imine bond) vibration of the incorporated complex moiety. The FT-IR spectra unambiguously prove that the desired surface modification of nanoparticles has been successfully done.

The degree of crystallinity of magnetic Fe_3O_4, Fe_3O_4@dopa, Fe_3O_4@dopa@MnL^1 and Fe_3O_4@dopa@FeL^1 was checked using PXRD measurements (Figure 4A). The PXRD data match well with the standard Fe_3O_4 sample. The same peaks are observed among the PXRD

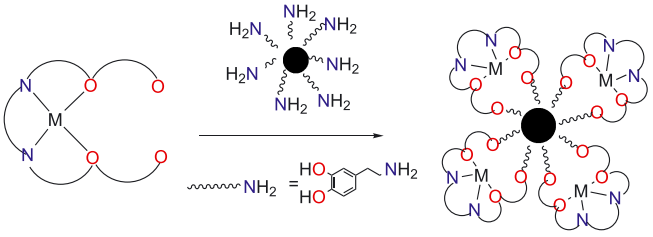

SCHEME 2 Schematic representation of the preparation of magnetically separable nanocatalysts, Fe_3O_4@dopa@ML^1 (M = Mn(III)/Fe(III))

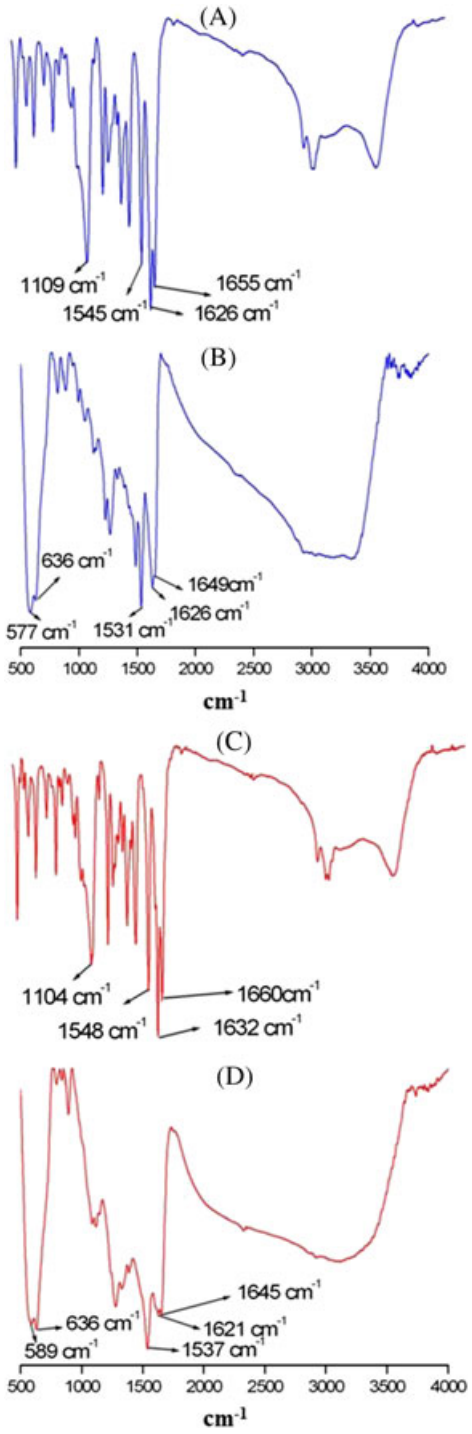

FIGURE 3 FT-IR spectra: (A) $[MnL^1]ClO_4$; (B) Fe_3O_4@dopa@MnL^1; (C) $[FeL^1]ClO_4$; (D) Fe_3O_4@dopa@FeL^1

patterns of Fe_3O_4@dopa, Fe_3O_4@dopa@MnL^1 and Fe_3O_4@dopa@FeL^1, indicating that the resultant nanoparticles contain pure Fe_3O_4 with a spinel structure and that the grafting process does not induce any phase change of Fe_3O_4 as previously found by our group for similar systems.[7] The solid-state UV spectra of Fe_3O_4, Fe_3O_4@dopa, Fe_3O_4@dopa@MnL^1 and Fe3O4@dopa@FeL^1 are depicted in Figure 4(B). The UV spectra of Fe_3O_4 and Fe_3O_4@dopa are very similar to those reported earlier.[7] MnL^1ClO_4 and FeL^1ClO_4 spectra have broad shoulders at

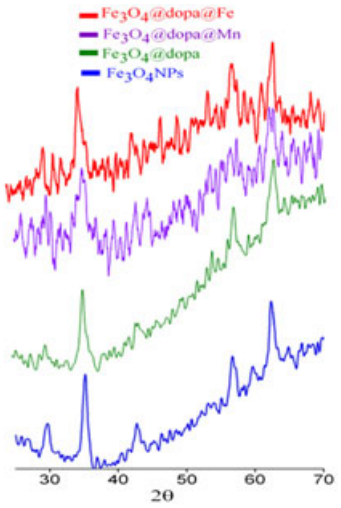

(A)

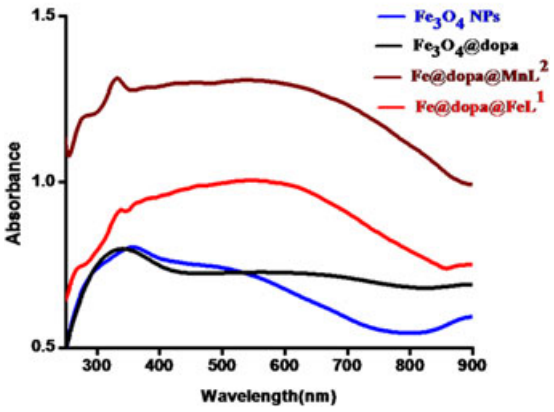

(B)

FIGURE 4 (A) PXRD spectra and (B) solid-state UV spectra of Fe_3O_4, Fe_3O_4@dopa, Fe_3O_4@dopa@MnL^1 and Fe_3O_4@dopa@FeL^1

ca 420 and 530 nm, respectively (Figure S1 and S2, supporting information). An increase of the absorbance clearly suggests the conjugation of MnL^1 and FeL^1 with Fe_3O_4@dopa.

Thermogravimetric analysis (TGA) was carried out for the verification of the successful surface modification of magnetic Fe_3O_4 and grafting of MnL^1ClO_4 and FeL^1ClO_4 on the surface of Fe_3O_4@dopa (Figure 5). The weight loss of Fe_3O_4 and Fe_3O_4@dopa is very similar as we reported earlier.[7] We observe 28 and 31% weight loss for Fe_3O_4@dopa@MnL^1 and Fe_3O_4@dopa@FeL^1, respectively. TGA results undoubtedly suggest that the enhanced weight loss is due to the increasing quantity of attached organic moiety from Fe_3O_4@dopa to Fe_3O_4@dopa@MnL^1 and to Fe_3O_4@dopa@FeL^1, similarly to the results described by our group earlier.[7]

SEM images of Fe_3O_4@dopa@MnL^1ClO_4 and Fe_3O_4@dopa@FeL^1ClO_4, presented in Figure 6, show morphologies quite different from those of Fe_3O_4-NPs and Fe_3O_4@dopa we reported in a previous work.[7] Both show agglomerated particles of larger size with respect to those reported and this alteration in morphology confirms the surface modification process.

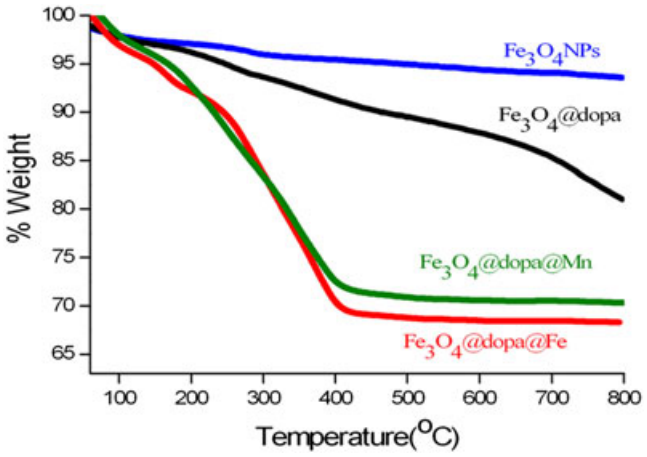

FIGURE 5 TGA curves of Fe_3O_4-NPs, Fe_3O_4@dopa, Fe_3O_4@dopa@MnL^1 and Fe_3O_4@dopa@FeL^1

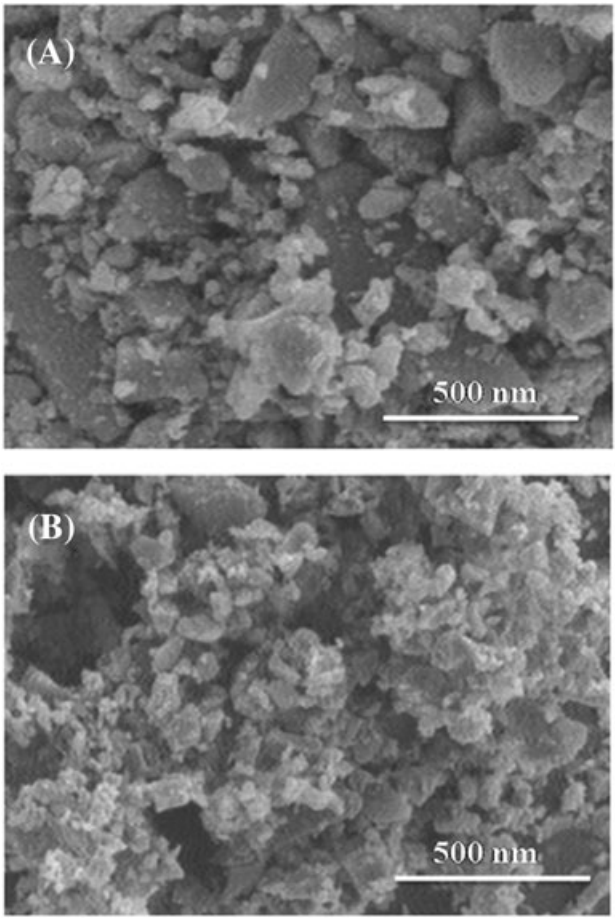

FIGURE 6 SEM images of (A) Fe_3O_4@dopa@MnL^1 and (B) Fe_3O_4@dopa@FeL^1

TEM images of Fe_3O_4@dopa@MnL^1 and Fe_3O_4@dopa@FeL^1 are shown in Figure 7. A close inspection of these images reveals that the magnetic nanoparticles are quasi-spherical with an average diameter of less than 10 nm. Here MnL^1ClO_4 and FeL^1ClO_4 are grafted on the surface of Fe_3O_4@dopa.

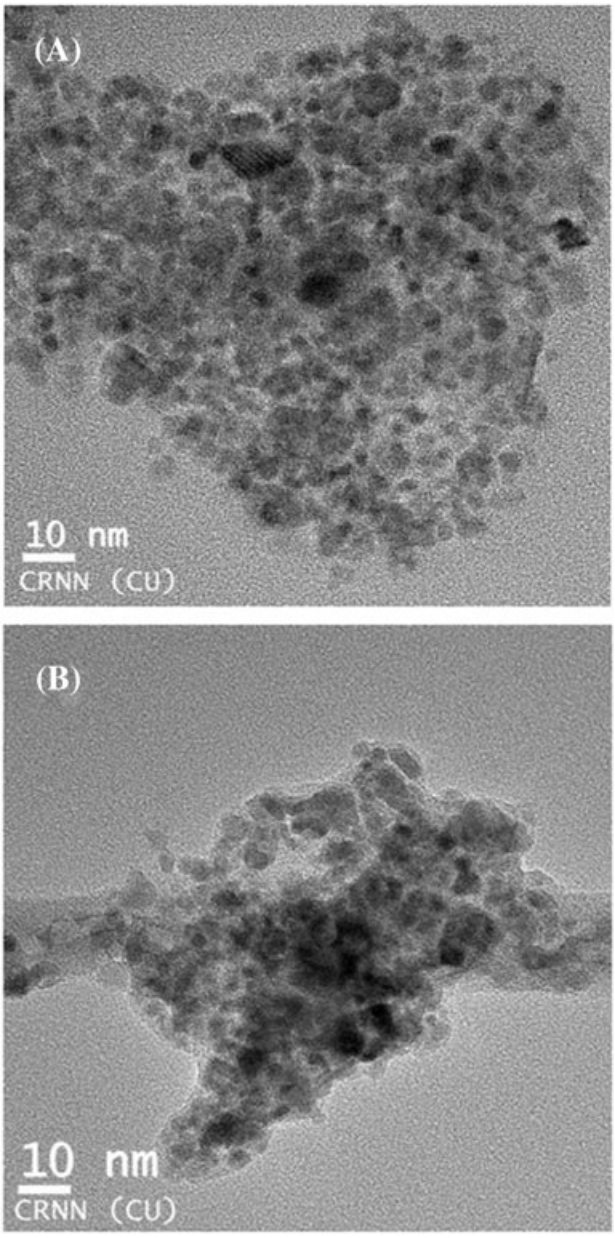

FIGURE 7 TEM images of (A) Fe_3O_4@dopa@MnL^1 and (B) Fe_3O_4@dopa@FeL^1

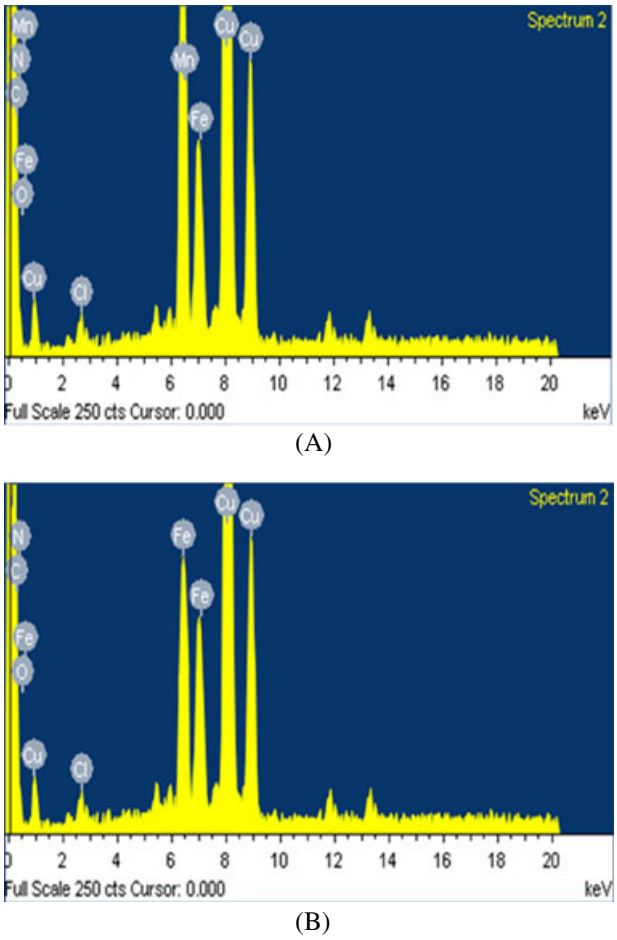

FIGURE 8 EDX spectra of (A) Fe_3O_4@dopa@MnL^1 and (B) Fe_3O_4@dopa@FeL^1

The energy-dispersive X-ray (EDX) spectra of Fe_3O_4@dopa@MnL^1 and Fe_3O_4@dopa@FeL^1 nanocatalysts are depicted in Figure 8. Fe and O signals are generated from the Fe_3O_4 nanoparticles and C signal is generated from dopamine. The well-defined peaks of iron and manganese in the EDX spectra of nanocomposites confirm the presence of MnL^1 and FeL^1 around the magnetic core. The copper (Cu) signals come from the coating material of the instrument.

3.6 | Epoxidation properties of Fe_3O_4@dopa@MnL^1 and Fe_3O_4@dopa@FeL^1

We evaluated the optimum reaction conditions in order to achieve the maximum epoxide yield from the heterogeneous catalyst, as already done for the homogeneous system. For this purpose a variable weight of Fe_3O_4@dopa@MnL^1 and Fe_3O_4@dopa@FeL^1 of between 50 and 200 mg was used per 3 mmol of (*E*)-stilbene. Enhancement in the yield of epoxide was observed when the amount of catalyst was increased from 50 to 100 mg but the yield remained the same with further increase of catalyst amount up to 200 mg. The reaction has also been studied by varying the amounts of terminal oxidant (PhIO) and time. Optimum epoxidation yield was obtained by using 3 mmol of PhIO and 6 h of stirring. At the end of the reaction, the catalyst was magnetically separated out and reused for further epoxidation. Here it is noteworthy that we did not find any leaching of catalyst during the epoxidation reaction. Again, the Fe_3O_4@dopa@MnL^1/Fe_3O_4@dopa@FeL^1-catalysed epoxidation of three different alkenes, (*E*)-stilbene, (*Z*)-stilbene and styrene, in CH_3CN with PhIO was studied and the results are presented in Table 3.

The magnetization behaviour of the Fe_3O_4-NPs, Fe_3O_4@dopa, Fe_3O_4@dopa@MnL^1 and Fe_3O_4@dopa@FeL^1 nanoparticles under an applied magnetic field is presented in Figure 9. The curves exhibit very similar phenomenon as we have observed earlier. Firstly, the decrease in the values of the saturation magnetization (M_s) from Fe_3O_4 nanoparticles (58.11 emu g^{-1}) to Fe_3O_4@dopa (39.22 emu g^{-1}) and to the final Fe_3O_4@dopa@MnL^3 and Fe_3O_4@dopa@FeL^6

TABLE 3 Epoxidation of alkenes catalysed by Fe_3O_4@dopa@MnL^1 and Fe_3O_4@dopa@FeL^1 in CH_3CN with PhIO[a]

Catalyst	Substrate	Conversion (%)	Yield (%)[b]	ee (%)[c]
Fe_3O_4@dopa@MnL^1	(*E*)-Stilbene	84	80	35
	(*Z*)-Stilbene	81	77 (*cis*: *trans* = 68: 32)	37
	Styrene	78	75	39
Fe_3O_4@dopa@FeL^1	(*E*)-Stilbene	45	41	25
	(*Z*)-Stilbene	50	48 (*cis*: *trans* = 75: 25)	27
	Styrene	34	31	35

[a]Catalyst (100 mg), alkene (2 mmol), PhIO (2 mmol) and CH_3CN (15 ml) stirred at room temperature for 2 h in air.

[b]Isolated epoxide yield.

[c]Determined by ^1H NMR (300 Hz) in the presence of Eu(hfc). Configuration not determined.

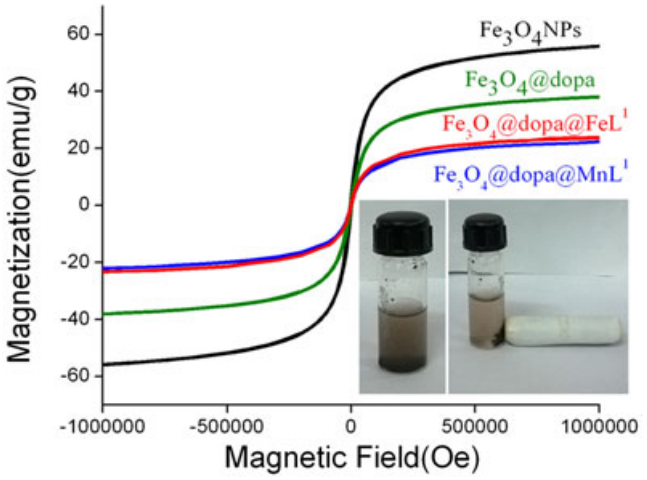

FIGURE 9 Magnetic curves of Fe_3O_4 NPs, Fe_3O_4@dopa, Fe_3O_4@dopa@MnL^1 and Fe_3O_4@dopa@FeL^1. Inset: image of the efficiency of the magnetic separation of the catalyst

nanocatalysts (19.29 and 18.99 emu g^{-1}, respectively) can be attributed to the gradual increase of diamagnetic organic materials from Fe_3O_4 to Fe_3O_4@dopa@MnL^3 and to Fe_3O_4@dopa@FeL^6. In addition, in comparison with the bulk magnetite nanomaterials that normally show a saturation magnetization value of 92 emu g^{-1}, the M_s value of the Fe_3O_4 nanoparticles is found to be much lower. Since the magnetization of a particle in an external field is a function of its size, the net magnetism exhibited by the final nanocatalysts is sufficiently good for an effective separation from the solution medium through the application of an external magnetic force.

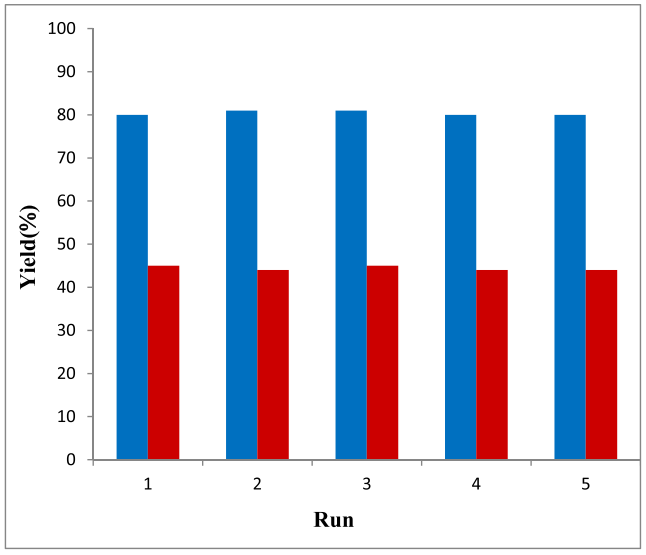

FIGURE 10 Reusability test of Fe_3O_4@dopa@MnL^1 (blue) and Fe_3O_4@dopa@FeL^1 (red) for the epoxidation of (*E*)-stilbene

3.7 | Reusability and characterization Fe_3O_4@dopa@MnL^1 and Fe_3O_4@dopa@FeL^1

The recycling efficiency of our synthesized magnetically separable heterogeneous nanocatalysts was also evaluated. A set of experiments was carried out by performing epoxidation of

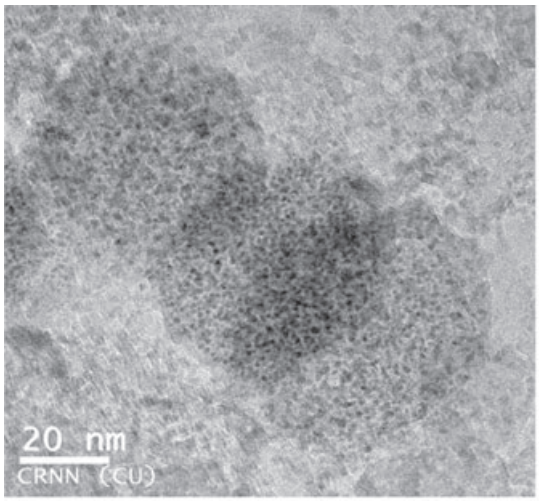

(A)

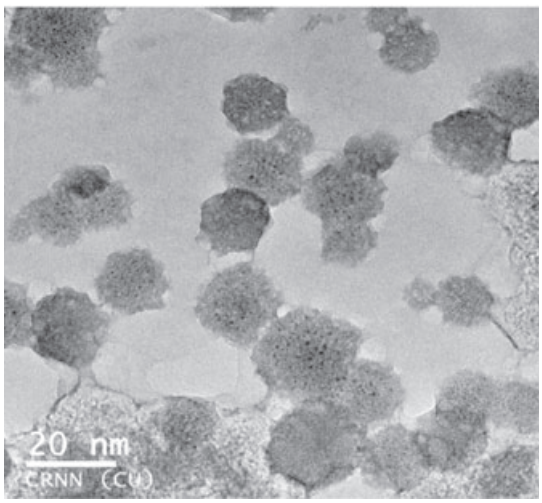

(B)

FIGURE 11 TEM images of used (A) Fe_3O_4@dopa@MnL^1 and (B) Fe_3O_4@dopa@FeL^1

(*E*)-stilbene catalysed by Fe_3O_4@dopa@MnL^1 and Fe_3O_4@dopa@FeL^1 nanocatalysts with the aim of examining their activity after five runs (Figure 10). After each run the catalysts were recovered solely by application of a magnet. Then these catalysts were washed with acetonitrile to remove any absorbed products and then dried. The used catalysts were further characterized using FT-IR spectroscopy (Figure S10, supporting information) and TEM (Figure 11). The results clearly indicate that the catalysts are stable with very good activity in the epoxidation reaction runs.

4 | CONCLUSIONS

In summary, we have found that ligand H_2L^3, formed from treatment of 2,6-diformyl-4-methylphenol with 1,1′-dimethylethylenediamine, renders the most efficient Mn(III) and Fe(III) Schiff base complexes for the epoxidation of alkenes both in homogeneous and heterogeneous catalysis. Density functional theory calculations confirm experimental results and suggest that the efficiency of the catalysts is related to the stability of Mn^V=O or Fe^V=O intermediates which form during the catalytic process in the presence of PhIO. Here we have adapted an economically workable and energy efficient catalytic process using MnL^1 or FeL^1 (L^1 comes from (*R*)-1,2-diaminopropane) complexes over magnetically separable nanoparticles for the selective epoxidation of alkenes at room temperature. The enantiomeric excess epoxide yields clearly show the retention of chirality at the backbone of the catalysts after addition with magnetically separable nanoparticles. The easy operation, the stability of catalysts, the use of cheap and mild magnetic nanoparticles as support, the easy recoverability and reusability of the catalysts, along with the high epoxide yield make them an environmentally acceptable and greener alternative to other reported catalytic systems for alkene epoxidation. Above all, we can consider that these novel catalytic systems would find applications in several other industrially significant catalytic processes as well as in general synthetic organic transformations due to their high enantiomeric excess yield.

ACKNOWLEDGMENTS

Financial support by the Science and Engineering Research Board (a statutory body under DST, New Delhi, India; F. no. SB/FT/CS-185/2013 dt. 30-06-2014) is gratefully acknowledged by T.C. We also thank DST, New Delhi, for providing single-crystal diffractometer facility at the Department of Chemistry, University of Calcutta, through DST-FIST programme.

REFERENCES

[1] G. D. Faveri, G. Ilyashenkoa, M. Watkinson, *Chem. Soc. Rev.* **2011**, *40*, 1722.

[2] Y. Zhu, Q. Wang, R. G. Cornwall, Y. Shi, *Chem. Rev.* **2014**, *114*, 8199.

[3] T. Katsuki, *Coord. Chem. Rev.* **1995**, *140*, 189.

[4] L. Canali, D. C. Sherrinton, *Chem. Soc. Rev.* **1999**, *28*, 85.

[5] C. Baleizão, H. Garcia, *Chem. Rev.* **2006**, *106*, 3987.

[6] Y. Kobayashi, S. Inukai, N. Asai, M. Oyamada, S. Ikegawa, Y. Sugiyama, H. Hamamoto, T. Shioiri, M. Matsugi, *Tetrahedron Asymm* **2014**, *25*, 1209.

[7] J. Adhikary, A. Datta, S. Dasgupta, A. Chakraborty, M. I. Menéndez, T. Chattopadhyay, *RSC Adv.* **2015**, *5*, 92634.

[8] D. Zhang, C. Zhou, Z. Sun, L. Z. Wu, C. H. Tung, T. Zhang, *Nanoscale* **2012**, *4*, 6244.

[9] M. Mazur, A. Barras, V. Kuncser, A. Galatanu, V. Zaitzev, K. V. Turcheniuk, P. Woisel, J. Lyskawa, W. Laure, A. Siriwardena, R. Boukherrouba, S. Szunerits, *Nanoscale* **2013**, *5*, 2692.

[10] S. Singamaneni, V. N. Bliznyuk, C. Binek, E. Y. Tsymbal, *J. Mater. Chem.* **2011**, *21*, 16819.

[11] V. Polshettiwar, B. Baruwati, R. S. Varma, *Green Chem.* **2009**, 11, 127.

[12] S. Shylesh, V. Schunemann, W. R. Thiel, *Angew. Chem. Int. Ed.* **2010**, *49*, 3428.

[13] M. B. Gawande, A. K. Rathi, I. D. Nogueira, R. S. Varma, P. S. Branco, *Green Chem.* **2013**, *15*, 1895.

[14] M. B. Gawande, P. S. Branco, R. S. Varma, *Chem. Soc. Rev.* **2013**, *42*, 3371.

[15] E. P. Talsi, K. P. Bryliakov, *Coord. Chem. Rev.* **2012**, *256*, 1418.

[16] T. Chattopadhyay, S. Islam, M. Nethaji, A. Majee, D. Das, *J. Mol. Catal. A* **2007**, *267*, 255.

[17] T. Chattopadhyay, D. Das, *J. Coord. Chem.* **2009**, *62*, 845.

[18] Collaborative Computational Project, Number 4, *Acta Crystallogr. D* **1994**, *50*, 760.

[19] Z. Otwinowski, W. Minor, *Methods Enzymol.* **1997**, *276*, 307.

[20] G. M. Sheldrick, *Acta Crystallogr. A* **2008**, *64*, 112.

[21] M. J. Frisch, G. W. Trucks, H. B. Schlegel, G. E. Scuseria, M. A. Robb, J. R. Cheeseman, G. Scalmani, V. Barone, B. Mennucci, G. A. Petersson, H. Nakatsuji, M. Caricato, X. Li, H. P. Hratchian, A. F. Izmaylov, J. Bloino, G. Zheng, J. L. Sonnenberg, M. Hada, M. Ehara, K. Toyota, R. Fukuda, J. Hasegawa, M. Ishida, T. Nakajima, Y. Honda, O. Kitao, H. Nakai, T. Vreven, Jr. J. A. Montgomery, J. E. Peralta, F. Ogliaro, M. Bearpark, J. J. Heyd, E. Brothers, K. N. Kudin, V. N. Staroverov, R. Kobayashi, J. Normand, K. Raghavachari, A. Rendell, J. C. Burant, S. S. Iyengar, J. Tomasi, M. Cossi, N. Rega, J. M. Millam, M. Klene, J. E. Knox, J. B. Cross, V. Bakken, C. Adamo, J. Jaramillo, R. Gomperts, R. E. Stratmann, O. Yazyev, A. J. Austin, R. Cammi, C. Pomelli, J. W. Ochterski, R. L. Martin, K. Morokuma, V. G. Zakrzewski, G. A. Voth, P. Salvador, J. J. Dannenberg, S. Dapprich, A. D. Daniels, Ö. Farkas, J. B. Foresman, J. V. Ortiz, J. Cioslowski, D. J. Fox, Gaussian, Inc., Wallingford, CT, **2009**.

[22] J. Tomasi, R. Cammi, *J. Comput. Chem.* **1996**, *16*, 1449.

[23] J. Tomasi, M. Persico, *Chem. Rev.* **1994**, *94*, 2027.

[24] S. Sahu, L. R. Widger, M. G. Quesne, S. P. de Visser, H. Matsumura, P. Moëne-Loccoz, M. A. Siegler, D. P. Goldberg, *J. Am. Chem. Soc.* **2013**, *135*, 10590.

[25] M. Katsuda, M. Mitani, Y. Yoshioka, J. Biophys, *Chem* **2012**, *3*, 111.

[26] A. B. Becke, *Phys. Rev. A* **1988**, *38*, 3098.

[27] A. B. Becke, *J. Chem. Phys.* **1993**, *98*, 5648.

[28] C. Lee, W. Yamg, R. G. Parr, *Phys. Rev. B* **1988**, *37*, 785.

[29] J. Adhikary, A. Guha, T. Chattopadhyay, D. Das, *Inorg. Chim. Acta* **2013**, *406*, 1.

[30] S.-C. Cheng, C.-W. Chang, H.-H. Wei, G.-H. Lee, Y. Wang, *J. Chin. Chem. Soc.* **2003**, *50*, 41.

SUPPORTING INFORMATION

Additional Supporting Information may be found online in the supporting information tab for this article.

How to cite this article: Chattopadhyay, T., Chakraborty, A., Dasgupta, S., Dutta, A., Menéndez, M. I., and Zangrando, E. (2016), A route to magnetically separable nanocatalysts: Combined experimental and theoretical investigation of alkyl substituent role in ligand backbone towards epoxidation ability, *Appl Organometal Chem*, doi: 10.1002/aoc.3663